On the path to bulk FeH$_2$: Synthesis and magnetic properties of amorphous iron (II) hydride

Leah Morris [a], Michel L. Trudeau [b], Martin R. Lees [c], John V. Hanna [c], David M. Antonelli [a,*]

[a] Sustainable Environment Research Centre, University of South Wales, Pontypridd CF37 4BD, United Kingdom
[b] IREQ, Hydro-Quebec, 1800 Boul. Lionel-Boulet, Varennes, Quebec J3X 1S1, Canada
[c] Department of Physics, University of Warwick, Gibbet Hill Road, Coventry CV4 7AL, United Kingdom

ABSTRACT

An amorphous Fe(II) hydride material approximating FeH$_2$ in composition (FeH$_{2-x}$R$_x$(Et$_2$O)$_y$ where R = mesityl) has been isolated as a bulk powder in the solid state. This was accomplished under moderate reaction conditions by the reaction of bis(mesityl) iron(II) in toluene and hydrogen gas at 100 bar and 298 K to give a 1:5 mixed phase amorphous material of Fe(0) and the iron (II) hydride. This represents an important advance because FeH$_2$ has never been synthesised in bulk form. The material shows ferromagnetic behaviour with a magnetic susceptibility of 1.25 Bohr magnetons per formula unit at 10 K.

© 2013 Elsevier B.V. All rights reserved.

1. Introduction

Knowledge of the chemistry of homoleptic transition metal hydride complexes is somewhat limited [1]. Iron hydride compounds in particular have in the past attracted research interest because both iron and hydrogen have a high abundance in the universe but homoleptic Fe hydrides are not well characterised, and FeH$_2$ in particular has never been synthesised in bulk form. The magnetic properties of iron compounds is an area of great interest, and in catalysis, iron hydride complexes play a pivotal role [2], for example as intermediates in hydrogenation [3] or hydrometalation [4] reactions. Due to the abundance of iron and its lower cost than precious metals, iron based complexes are being investigated as an alternative to precious metal based system for C–C and C–heteroatom bond formation in organic syntheses [5]. By understanding the reaction between H$_2$ and iron and learning more about the structure and properties of FeH$_2$ may lead to improvements in the properties of iron based catalysts. The study of iron hydride compounds is also important in the understanding of hydrogen embrittlement of iron metal, which can have a negative effect on its mechanical properties [6].

Iron hydrides also play an important role in the development of metal hydrides for energy storage. The magnesium iron hydride, Mg$_2$FeH$_6$ for example stores gravimetrically 5.5 wt% of hydrogen and could be used as a reversible system for storing thermal energy [7]. In previous work we reported hydrogen storage materials such as chromium hydrazide hydrides [8] that use the Kubas interaction as the hydrogen binding mechanism. The Kubas interaction typically have hydrogen binding enthalpies that fall into the range of 20–30 kJ/mol range that is required for room temperature hydrogen storage [9]. Recently we extended this work to the homoleptic titanium hydride gel TiH$_3$ [10,11]. As iron is less expensive than earlier transition metals such as titanium and vanadium, it is possible that a polymeric FeH$_2$ compound containing hydride ligands as bridging features, could be used for room temperature hydrogen storage on the basis that each Fe in FeH$_2$ could bind up to 4 H$_2$ on the basis of the eighteen electron rule.

At ambient temperature and atmospheric pressure, solid metallic iron does not react with hydrogen. The iron monohydride, FeH is a compound found in the sun and the atmosphere of cool stars [12]. FeH has been isolated above the boiling point of iron as a gas or by trapping the molecule in a cryogenic noble gas matrix [13]. In 1991 the formation of iron hydride from reaction of iron metal and fluid hydrogen at pressures up to 62 GPa was reported. X-ray diffraction measurements were carried out during the reaction and the stoichiometry was determined was close to that of FeH [14]. In general, transition metal dihydrides are rare in bulk form and not well characterised. The iron dihydride, FeH$_2$ was first identified by the reaction of Fe atoms and hydrogen in low temperature matrices [15,16] and later the molecule was formed in an electric discharge from iron pentacarbonyl and hydrogen in helium as a carrier [17,18]. Due to the difficulty in synthesising and

* Corresponding author. Tel.: +44 01443 654691.
  E-mail addresses: leah.morris@southwales.ac.uk (L. Morris), david.antonelli@southwales.ac.uk (D.M. Antonelli).

isolating bulk FeH_2 under ambient conditions there is limited knowledge of its physical and magnetic properties. In light of this we attempted a new route towards FeH_2 based on the well-known hydrogeneolysis of transition metal complexes [19].

2. Materials and methods

2.1. General

All chemicals were purchased from Sigma–Aldrich and used without further purification. Dry diethyl ether, tetrahydrofuran (THF) and toluene were obtained using an MBraun Solvent Purification System, which feeds directly into an MBraun glovebox. Manipulations were performed in an Argon glove box and on a Nitrogen Schlenk line. Reactions with hydrogen were carried out in solution using a stainless steel PARR hydrogenation vessel and in the solid state using a Hy-Energy PCT-Pro Sieverts instrument. Grade 6 hydrogen purchased from Air Liquide was used for synthesis.

2.2. Syntheses

2.2.1. Preparation of bis(mesityl) iron (II)[20]
$FeCl_2$ (5.0416 g, 39.77 mmol) was stirred in 50 mL of dry THF to give a pale orange suspension. To this 79.54 mmol, 79.54 mL of a 1.0 M solution of mesityl magnesium bromide in THF was added drop wise and the reaction mixture rapidly turned dark red/brown. After stirring for 30 min at room temperature, 60 mL of dioxane was added to precipitate the magnesium salts and the reaction continued stirring overnight. After leaving to stand for a couple of hours, the reaction was filtered to give a white precipitate. The red dark filtrate was concentrated *in vacuo* and recrystallised from diethyl ether to give a dark red/purple crystalline solid (4 g, 34%).

2.2.2. Preparation of iron(II) alkyl hydride
Bis(mesityl) iron (II) (3.5 g, 11.89 mmol) was stirred in 150 mL of dry toluene to give a dark red solution and transferred to a stainless steel hydrogenation vessel. The vessel was charged with 100 bar for H_2 and the reaction stirred for 24 h at 298 K. The reaction mixture turned black after 24 h and was filtered to give a black solid and colourless filtrate. The black solid was dried *in vacuo* at 100 °C to give an air-moisture sensitive black powder (0.596 g) (FeH-100). The black powder was transferred to a stainless steel PCT-Pro sample holder and charged with 85 bar hydrogen at 150 °C for two hours, followed by evacuation at 100 °C for 2 h before being allowed to cool to room temperature to give a black powder (FeH-85).

2.3. Characterisation

Infrared spectroscopy was conducted on a Perkin Elmer Spectrum RX1 using KBr. Prior to analysis the IR grade KBr was oven dried overnight at 120 °C to remove any residual water. A blank sample of KBr was ground in an oven-dried pestle and mortar in the glovebox and then compressed in air to form a disc. A background was taken of the blank KBr disc. Approximately 5 mg of sample was ground with 200 mg KBr in the glovebox and then compressed in air quickly to form a disc. The spectrum of KBr was subtracted from the IR of the sample. Nitrogen adsorption and desorption data were collected at 77 K on a Micromeritics ASAP 2020. The Powder X-ray Diffraction (PXRD) analysis was done using two different setups. A small amount of powder was placed in small capillaries (1 mm or 0.2 mm in diameter) and the XRD spectrum was taken using a Bruker Discover diffractometer with a Vantec 500 2D detector using Co Kα radiation. The X-ray beam was limited using a 0.2 mm collimator. Larger amounts of powder were place inside a glove box on a thin glass plate using 2-sided tape. This glass plate was then positioned in an O-ring sealed X-ray transparent holder. The X-ray spectrum was taken using a Bruker DaVinci diffractometer with Cu Kα radiation. The XPS analysis was performed using a PHI-5500 spectrometer using monochromated Al Kα radiation. The positions of the peaks were referenced to surface C–C or C–H bound at 284.8 eV. The powder was placed on the XPS holder inside an Ar glove box and transferred under Ar to the XPS intro chamber without any exposure to air. For insulating materials, an electron-flooding gun was used to compensate the surface charges. The different chemical contributions for each spectrum were obtained using CasaXPS. The thermogravimetric analysis (TGA) and differential thermal analysis (DTA) was done in a STA 449C analyser from Netzsch under a flow of dried air at 10.00 °C/min up to 650 °C. Argon was also used to protect the balance section. High resolution Transmission Electron Microscopy (HRTEM) was performed on an HD-2700 dedicated Scanning Transmission Electron Microscope (STEM) from Hitachi, with a cold field emitter equipped with a CEOS Cs corrector and operated at 200 kV. Some powder was placed onto a copper grid covered with a carbon layer having regular hole with a diameter of 1.2 μm. The powder was deposited on the grid inside a Ar glove box at 0.3 ppm of O_2. After that, the grid was mounted on a TEM holder having a special cover that isolates the sample from the air. The holder was then placed in the TEM goniometer and the sample region was evacuated a couple of times before retracting the cover and inserting the sample inside the TEM. Observation was

made in three different modes: Bright Field (BF), High Angle Annular Dark Field (HAADF) and Secondary Electron (SE). Magnetisation measurements were carried out in a Quantum Design MPMS-5XL SQUID magnetometer. Magnetisation (*M*) versus applied field (*H*) hysteresis loops were collected at 10 and 280 K in applied fields of up to 50 kOe. (4 MAm-1). Magnetisation versus temperature (*M* vs *T*) data was collected between 5 and 280 K (or 350 K, depending on the data set) in an applied magnetic field of 100 Oe ($8\ kAm^{-1}$). For the zero-field-cooled warming (ZFCW) curve, the sample was cooled from room temperature in zero applied field to the base temperature of 5 K. The magnetic field was then applied and the temperature dependence of the magnetisation measured. The field-cooled cooling (FCC) curve was collected on cooling in the same applied field.

2.4. Hydrogen adsorption measurements

Hydrogen adsorption isotherms were obtained by using a computer controlled gas sorption Sieverts apparatus manufactured by Hy-Energy. High purity hydrogen (Grade 6, 99.9999% purity) purchased from Air Liquide was used. Stainless steel spacers were added to the sample holder along with the material to reduce excess void space. The void space of the sample was calculated by performing a helium volume calibration at 298 K. Excess hydrogen storage measurements on a 100 mg standard AX-21 sample (0.81 wt.% at 100 bar and 298 K) were performed to ensure correct functioning of the instrument (Fig. S5). These measurements are all necessary to ensure the accuracy of the isotherms. The reported gravimetric hydrogen storage capacity of Carbon AX-21 at 298 K is 0.3 wt% at 35 bar [21]. This corresponds to 0.85 wt% at 100 bar which gives an error in our measurement of ±0.04 wt% ($(0.65 - 0.6) \times 100/70$) at 100 bar H_2 for a 100 mg sample size of AX-21. This equates to 0.04 mg H_2, or 0.02 mmol H_2.

3. Results and discussion

In this study we report a facile route to iron(II) alkyl hydride using mild reaction conditions. Bis(mesityl) iron(II) was prepared following the literature procedure [20] and dissolved in toluene to give a dark red solution. The solution was stirred in a high-pressure stainless steel vessel charged with 100 bar of hydrogen. After 24 h stirring at room temperature, the reaction mixture was filtered to give a black precipitate and colourless filtrate. The colourless filtrate indicates complete reaction of the bis(mesityl) iron(II) precursor with hydrogen. The precipitate was dried *in vacuo* to give an air-moisture sensitive black powder (FeH-100). The mechanism we propose is that the mesityl ligands of bis(mesityl)iron (II) are replaced by hydride ligands using the well known hydrogenolysis reaction of transition metal complexes M–R to form M–H species and R–H [19]. The proposed reaction is shown in Scheme 1. Further reaction with hydrogen was carried out in the solid state using a Hy-Energy PCT-Pro Sieverts instrument. The FeH-100 powdered sample was loaded into the stainless steel holder and charged with 85 bar H_2 at 150 °C for 2 h, followed by evacuation at 100 °C to remove any remaining hydrocarbon via hydrogenolysis to give material FeH-85.

The infrared spectrum of FeH-85 is shown in Fig. 1. There are C–H stretches at 2919 and 2961 cm^{-1} and an aromatic C=C stretch at 1485 cm^{-1} that arise from the presence of mesityl ligands that have not been fully cleaved by hydrogenolysis. Diagnostic transition metal-hydride stretches normally appear in the $1900 \pm 300\ cm^{-1}$ region and can be variable in intensity [19]. Fe–H stretches can be observed at 1600 and 1636 cm^{-1} in the IR for matrix isolated FeH_2 molecules at cryogenic temperatures [15,16] but are partially obscured by the presence of matrix isolated water in the original study. In KBr, water comes at 3300 and 1647 cm^{-1}. The stretch in the spectrum of FeH-85 at 1630 cm^{-1} corresponds to ambient water absorbed by the KBr disc during the rapid transfer step from the glove box to IR apparatus. Since the Fe–H in the original study comes in this region, it is possible that there is an Fe–H stretch contributing to this band at 1630 cm^{-1} in the IR. However there is also a weaker band at 1780 cm^{-1} which is not obscured by any other bands and can thus be assigned with great confidence to an Fe–H stretch since there are no other expected absorbances in this region. There are also C–O stretches at 1028 and 1077 cm^{-1} which can be assigned to coordinated diethyl ether
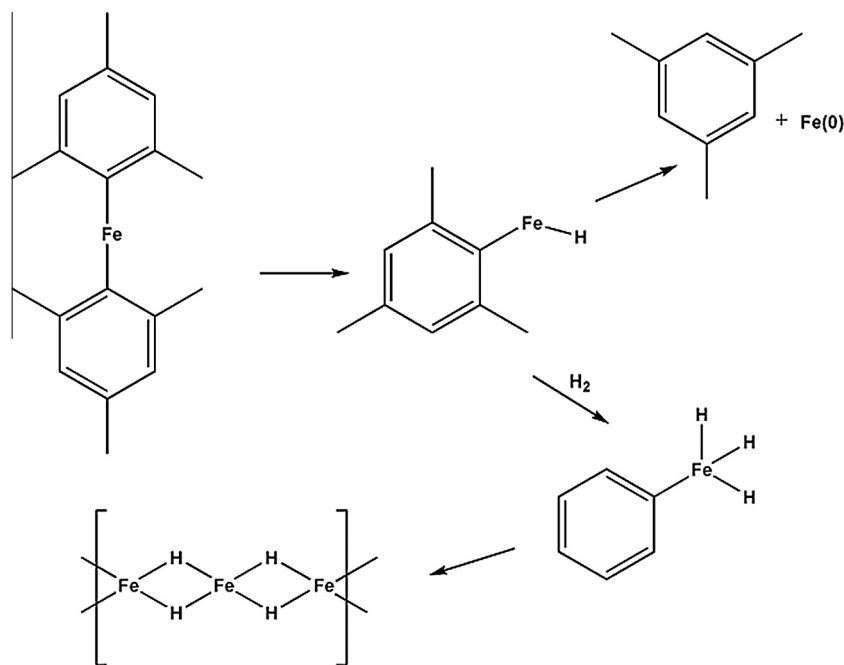
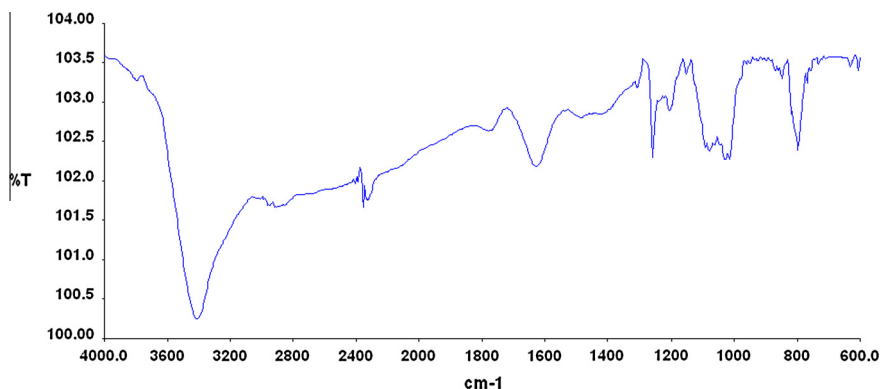**Scheme 1.** Proposed reaction of bis(mesityl) iron(II) and hydrogen.

Fig. 1. Infrared spectra of FeH-85.

which has been carried through into the final material from diethyl ether of crystallisation from the preparation of $Fe_2(mes)_4$.

Nitrogen adsorption–desorption isotherms of FeH-100 and FeH-85 were recorded at 77 K and are shown in Figs. S1 and S2 respectively. The material FeH-100 has a Brunauer–Emmett–Teller (BET) surface area of 14 m^2/g. After solid-state hydrogenation at 85 bar H_2 and 150 °C, the BET surface area of FeH-85 decreases to 7 m^2/g. This is likely due to the loss of hydrocarbon from the material by hydrogeneolysis causing densification of the structure. The isotherms for both FeH-100 and FeH-85 can be classified as Type II and the presence of hysteresis between the adsorption and desorption isotherms indicate that the material possesses some mesoporosity. As there is only a small increase in slope between 0 and 0.1 P/P_0 we can assume that both materials have none or very little microporosity. The increasing slope between 0.8 and 1.0 P/P_0 arises from textural porosity.

The powder X-ray diffraction (PXRD) of FeH-85 is shown in Fig. S3. The reflections in the 2θ region of 0–30° correspond to the glass sample holder and the glue used to fix the powdered sample to the glass plate. The reflections in the 2θ region of 30–85° corresponds to some metallic iron that was formed as a side product.

The Fe(II) hydride species does not give rise to any reflections in the PXRD meaning that the material is largely amorphous with the presence of some metallic iron.

X-ray Photoelectron Spectroscopy (XPS) of FeH-85 performed with rigorous exclusion of air is shown below in Fig. 2. In the Fe 2p3/2 region, there are two emissions at 707.2 and 710.2 eV. The emission at 707.2 eV corresponds to metallic Fe(0) [22]. The emission at 710.2 eV can be attributed to Fe(II) hydride species as the emission is close to that observed for Fe(II)O [23]. In the preparation of Fe-85 the handling of reagents was strictly done under inert conditions and grade 6 hydrogen was used for the preparation of Fe-100 and again for solid state hydrogenation to give FeH-85. Therefore the only likely product formed from the reaction of bis(mesityl)iron (II) and hydrogen that could give rise to an Fe(II) emission is an Fe(II) hydride. Also the room temperature reaction of Fe(0) and diethyl ether (carried through into the final material from diethyl ether of crystallisation of bis(mesityl)iron (II)) is not known. We would expect that the emission for FeO and Fe(II) hydride to come in a similar region of the XPS spectrum. The emission for the Fe(II) species is broad suggesting multiple environments expected from an amorphous solid and is significantly larger in
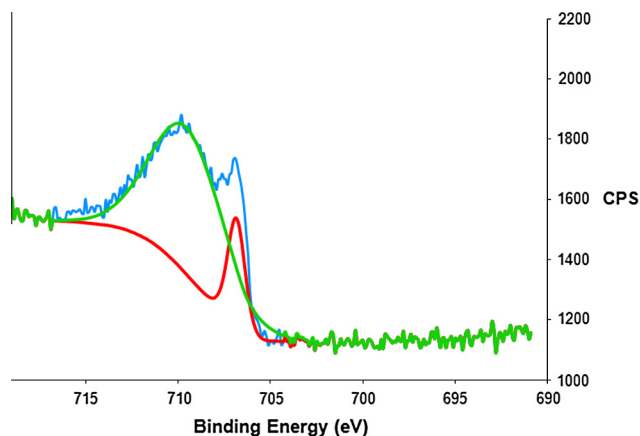
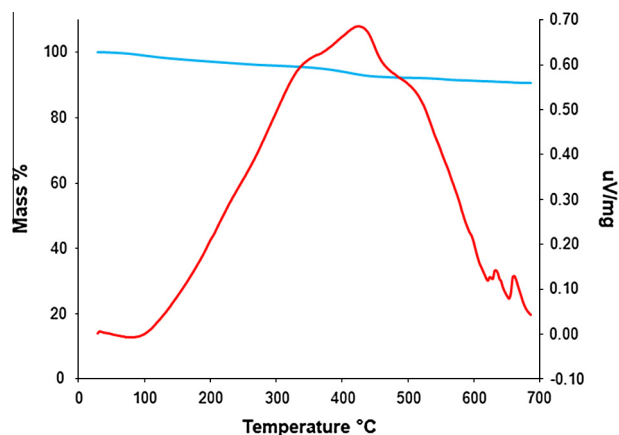**Fig. 2.** Iron 2p1/2 and 2p3/2 region of XPS Spectrum of FeH-85.

Fig. 3. TGA (blue) and DTA (red) curves of FeH-85. (For interpretation of the references to colour in this figure legend, the reader is referred to the web version of this article.)

intensity than the Fe(0) emission indicating that the Fe(II) hydride is the more prominent phase in this material. Since heating Fe-H150 at 150 °C did not lead to any change in the amount of Fe(0) present, the Fe(0) must be formed as a side-product in the synthesis. The formation of Fe(0) rules out concerted hydrogenation of the Fe—C bond in favour of oxidative addition of H_2 to form the Fe (IV) species. Thus, in reaction Scheme 1 the formation of Fe(0)

can be rationalised by oxidative addition of H_2 to bis mesitylene iron followed by reductive elimination of two equivalents of mesitylene and FeH_2 can only be formed by reductive elimination of mesitylene from $Fe(mesityl)H_3$, as further hydrogenation of metallic Fe does not to lead to FeH_2.

Thermogravimetric analysis (TGA) was performed to determine the quantity of remaining hydrocarbon present in the material. A thermo-gravimetric plot of FeH-85 is shown in Fig. 3. At the maximum heat the material retained 90.62% of its original mass. The thermogravimetric curve of FeH-85 shows at 428 °C there is a loss of 7% mass which is due to the combustion of residual mesityl ligand from the material and residual diethyl ether present. This is also evident in the in the DTA curve where there is an exothermic peak at 429 °C. From analysis of the material by IR and TGA we propose that the formula of the Fe(II) amorphous phase is $FeH_{2-x}R_x(Et_2O)_y$ where x and y are small due to the 90.62% retention of mass. On the basis of the XPS ratio of 5:1 and the TGA data the material is roughly 75% FeH_2 by mass, neglecting of course conversion of Fe species to oxides and hydroxides in the TGA combustion process.

To further study the structure of the material scanning transmission electron microscopy (STEM) of FeH-85 was carried out. Two different phases in the material were observed, which is consistent with the XPS that shows there are two different oxidation states of iron species in the material. The crystalline Fe(0) phase was observed and is shown at a scale of 2 and 5 nm in Fig. S4. The amorphous phase consists of cauliflower-like structures as shown below at a scale of 10 and 20 nm in Fig. 4. The amorphous phase shown by the STEM is from the Fe(II) hydride component which is consistent with the PXRD, in that the diffraction pattern for crystalline Fe(0) was observed and the amorphous Fe(II)hydride phase did not give rise to any reflections. Transfer of the Fe-85 material from an Argon glovebox to the transmission electron microscope was done under strict inert conditions so we can be confident that the amorphous phase shown in Fig. 4 is from the amorphous Fe(II) hydride phase and not due to reaction of the Fe(0) phase with oxygen.

The magnetometry data shown in Figs. 5–7 indicate ferromagnetic behaviour and possible superparamagnetic characteristics, with a magnetic ordering temperature in excess of 350 K. Figs. 5 and 6 illustrate the magnetisation (M) versus applied field (H) curves that were acquired at 10, 150, and 285 K. The $M(H)$ curves saturate in applied fields above ~1.6MA/m (i.e. $\mu_0 H = 2$ T) and the saturation magnetisation decreases from 1.25 to 1.18 Bohr magnetons per formula unit over this temperature range.

The magnetic moment per Fe atom is less than the spin only $4\mu_B$ Bohr magnetons expected for a Fe^{2+} ion or ~$2.2\mu_B$ per Fe atom or 221.7 Am^2/kg for bulk Fe [24]. Reduced moments have been
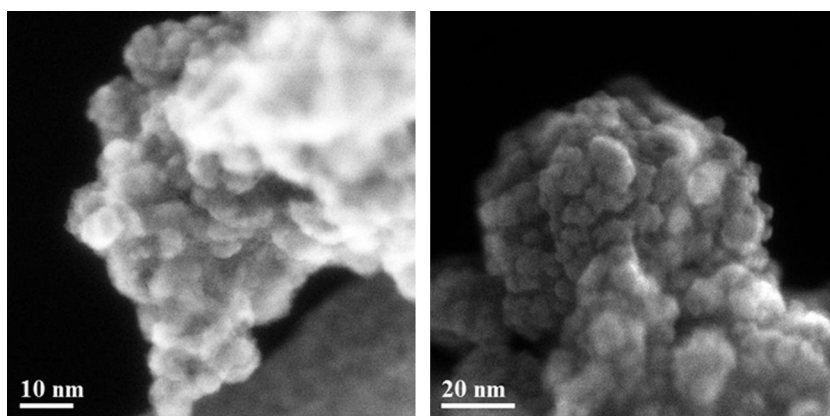

Fig. 4. Left: SEM image of the amorphous Fe(II) region of FeH-85 at a scale of 10 nm. Right: SEM image of the amorphous Fe(II) region of FeH-85 at a scale of 20 nm.
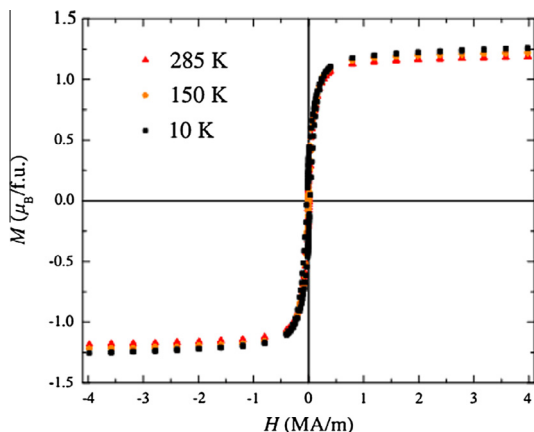
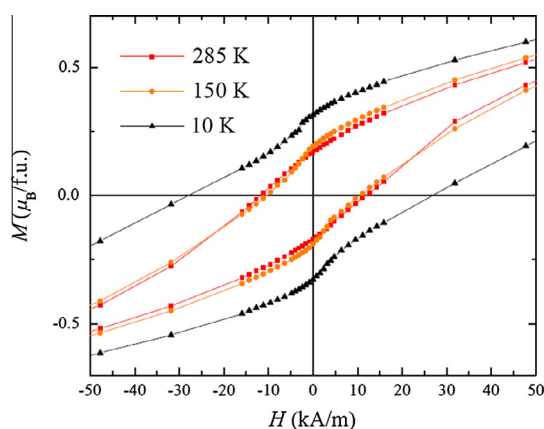**Fig. 5.** Magnetisation (M) versus applied field (H) of FeH-85 at 10, 150 and 285 K.

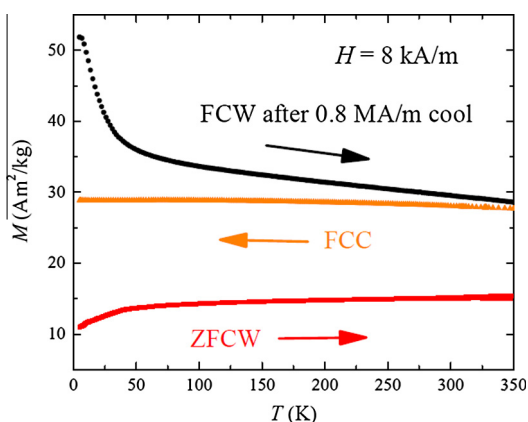**Fig. 6.** Magnetisation (M) versus applied field (H) of FeH-85 at 10, 150 and 285 K.

Fig. 7. Magnetisation (M) versus temperature (T) of FeH-85.

reported for ultra-fine iron particles [25] and amorphous iron [26] and the saturation magnetisation of Fe nanoparticles is typically lower than that of bulk Fe, ranging from 134 to 183 Am^2/kg, depending on the grain size and morphology [27]. On the basis that FeH-85 is a 5:1 mixture of Fe(II) to Fe(0), then the contribution of magnetisation from the amorphous Fe(II) phase is estimated to be 105 Am^2/kg or $\sim 1\mu_B$ per Fe, lower than that observed for bulk Fe(0). The low field magnetic behaviour shown in Fig. 6 demonstrates that all $M(H)$ curves are hysteretic and the remnant

magnetisation and coercive field both decrease with increasing temperature.

The associated M versus temperature (T) behaviour in Fig. 7 shows considerable field history. During this experiment the sample was initially cooled in zero field, a field of 8 kA/m ($\mu_0 H = 0.01$ T) was applied, and the red (ZFCW) curve was measured; then 0.8 MA/m was applied at 350 K to saturate the sample which was then cooled to base. A field of 8 kA/m was again applied and the sample warmed to give the black (FCW) curve. Finally the sample was re-cooled in this same 8 kA/m field to yield the orange (FCC) curve.

In order to probe the possible applications to hydrogen storage, hydrogen PCT adsorption–desorption isotherms were recorded at 298 K and the isotherms are shown in Fig. S5. The material shows limited hydrogen storage performance at room temperature, reaching 0.25 wt% at 142 bar and 298 K. The isotherm is linear and does not reach saturation indicating that improved performance may be observed at higher pressures. This type of behaviour is different to that seen by hydrogen storage materials that use physisorption as the hydrogen binding mechanism and has been seen previously in chromium, vanadium and titanium materials previously published by our group [8,28,29]. There is some hysteresis between the adsorption and desorption isotherms indicating that there is a small kinetic barrier to overcome in order to fully desorb the material.

4. Conclusion

The reaction of bis(mesityl) iron(II) and hydrogen gas at 298 K, followed by further solid state hydrogenation at 150 °C has afforded a rare Fe(II) bulk hydride material approximating FeH$_2$ consisting of an amorphous FeH$_{2-x}$R$_x$(Et$_2$O)$_y$ phase strongly suggested by IR and XPS. A small amount of crystalline Fe(0) impurity was also observed by PXRD and STEM imaging. The material shows ferromagnetic behaviour with a magnetic susceptibility of 1.25 Bohr magnetons per formula unit. Although this material exhibited disappointing room temperature hydrogen storage properties, the synthesis of an Fe(II) hydride species in the solid state will help to further understand the chemistry and physical properties of homoleptic iron hydrides which in the future could contribute to improvements in the use of Fe hydrides in catalysis and energy storage. The catalytic applications of this material are currently under exploration.

Appendix A. Supplementary material

Supplementary material associated with this article can be found, in the online version, at http://dx.doi.org/10.1016/j.jallcom.2013.12.099.

References

[1] R.B. King, Coord. Chem. Rev. 200–202 (2000) 813–829.
[2] H. Nakazawa, M. Itazaki, Fe–H complexes in catalysis, in: B. Plietker (Ed.), Iron Catal., Springer, Berlin, Heidelberg, 2011, pp. 27–81.
[3] M.A. Esteruelas, L.A. Oro, Chem. Rev. 98 (1998) 577–588.
[4] J.Y. Wu, B. Moreau, T. Ritter, J. Am. Chem. Soc. 131 (2009) 12915–12917.
[5] C. Bolm, J. Legros, J. Le Paih, L. Zani, Chem. Rev. 104 (2004) 6217–6254.
[6] R.A. Oriani, J.P. Hirth, M. Smialowski, Hydrogen Degradation of Ferrous Alloys, Noyes Publications, 1985.
[7] M. Felderhoff, B. Bogdanovic, Int. J. Mol. Sci. 10 (2009) 325–344.
[8] H.V. Mai, T.K.A. Hoang, A. Hamaed, M. Trudeau, D.M. Antonelli, Chem. Commun. 46 (2010) 3206.
[9] T.K.A. Hoang, D.M. Antonelli, Adv. Mater. 21 (2009) 1787–1800.
[10] D. Antonelli, Novel metal hydrides and their use in hydrogen storage applications, 2013. (WO2013088170 (A1)).
[11] T.K.A. Hoang, L. Morris, D. Reed, D. Book, M.L. Trudeau, D.M. Antonelli, Chem. Mater. (2013).
[12] P.K. Carroll, P. McCormack, S. O'Connor, Astrophys. J. 208 (1976) 903–913.

[13] G.V. Chertihin, L. Andrews, J. Phys. Chem. 99 (1995) 12131–12134.
[14] J.V. Badding, R.J. Hemley, H.K. Mao, Science 253 (1991) 421–424.
[15] G.A. Ozin, J.G. McCaffrey, J. Phys. Chem. 88 (1984) 645–648.
[16] R.L. Rubinovitz, E.R. Nixon, J. Phys. Chem. 90 (1986) 1940–1944.
[17] H. Körsgen, P. Mürtz, K. Lipus, W. Urban, J.P. Towle, J.M. Brown, J. Chem. Phys. 104 (1996) 4859–4861.
[18] H. Körsgen, W. Urban, J.M. Brown, J. Chem. Phys. 110 (1999) 3861–3869.
[19] H.D. Kaesz, R.B. Saillant, Chem. Rev. 72 (1972) 231–281.
[20] A. Klose, E. Solari, R. Ferguson, C. Floriani, A. Chiesi-Villa, C. Rizzoli, Organometallics 12 (1993) 2414–2416.
[21] Chahine, Bernard, Assessment of hydrogen Storage on different carbons – NN0094v.pdf, (n.d.).
[22] S. Sinha, S. Badrinarayanan, A.P.B. Sinha, J. Common Metal 125 (1986) 85–95.
[23] G.C. Allen, M.T. Curtis, A.J. Hooper, P.M. Tucker, J. Chem. Soc. Dalton Trans. (1974) 1525–1530.
[24] H. Danan, A. Herr, A.J.P. Meyer, J. Appl. Phys. 39 (1968) 669–670.
[25] S.U. Jen, C.Y. Lee, Y.D. Yao, K.C. Lee, J. Magn. Magn. Mater. 96 (1991) 82–88.
[26] M.W. Grinstaff, M.B. Salamon, K.S. Suslick, Phys. Rev. B. 48 (1993) 269–273.
[27] M. Kamata, H. Kura, M. Takahashi, T. Ogawa, T. Tanaka, IEEE Trans. Magn. 48 (2012) 3944–3946.
[28] T.K.A. Hoang, L. Morris, J.M. Rawson, M.L. Trudeau, D.M. Antonelli, Chem. Mater. 24 (2012) 1629–1638.
[29] T.K.A. Hoang, L. Morris, J. Sun, M.L. Trudeau, D.M. Antonelli, J. Mater. Chem. A 1 (2013) 1947–1951.